A ZigBee-Based Wireless Sensor Network Node for Ultraviolet Detection of Flame

Pedro Cheong, *Student Member, IEEE*, Ka-Fai Chang, *Member, IEEE*, Ying-Hoi Lai, Sut-Kam Ho, Iam-Keong Sou, and Kam-Weng Tam, *Senior Member, IEEE*

***Abstract*—This paper describes a ZigBee-based wireless sensor network node for the ultraviolet (UV) detection of flame. The sensor node is composed of a ZnSSe UV photodetector, a current-sensitive front end including a high-gain current-to-voltage amplifier with 120 dB and a logarithm converter, and a transceiver operated at a 2.4-GHz industrial, scientific, and medical band. A passive photodetector is designed to have a cutoff at 360 nm and convert the UV emission of flame into picoamperes. Including mixed signal processing and ZigBee transmission, the speed of flame detection is as fast as 70 ms. The sensor node consumes only an average of 2.3 mW from a 3.3-V supply. The performance of a prototype sensor node was verified when the luminous flame was imaged onto the sensor node with different angles ranging from -30° to 30° and distances of 0.1, 0.2, and 0.3 m enabling effective fire safety applications.**

***Index Terms*—Flame analysis, ultraviolet (UV) detector, wireless sensor network (WSN), ZigBee.**

I. Introduction

FIRE is considered as one of the serious threats in our daily life with fast spreading speed and totality of property destruction. Low cost, reliable, and wide coverage fire alarm systems are indispensable in industry to protect the equipment and assets. The damage can be mitigated if fire is detected as soon as possible. The most commonly used fire detector in the fire safety sector is the smoke detector even if they always have false alarms. Some estimates are as high as 11 to 1 for the ratios of false to actual alarms. Their applications are also limited in a confined area as the smoke concentration may be diluted in a large monitoring area, which delays or even worst desensitizes the alarm triggering. Being able to compensate the aforementioned disadvantages of smoke detectors, optical flame detectors offer higher reliability, good long-term stability, and prompt response to accidents. Flame detectors that use optical sensors working at specific spectral ranges to record the incoming electromagnetic emission at the selected wavelengths include infrared (IR) [1]–[3], visible [2] and ultraviolet (UV) [1], [2], [4]–[6]. UV-only flame detectors work with wavelengths shorter than 400 nm. They detect flames at a high speed of 3–4 ms due to the UV high-energy radiation emitted by fires and explosion at the instant of their ignition. UV/IR detectors compare the threshold signal in two spectral ranges and their ratio to each other to confirm the reliability of the fire signal, minimizing false alarms. However, available UV flame detectors [7] are based on the Geiger–Müller counter, a quartz tube filled with an inert gas that conducts electricity when a photon of wavelength between 185 and 260 nm of a flame temporarily makes the gas conductive. This type of flame detector is indeed bulky and expensive, operates at high voltage, has short lifetime, and optically interferes with others in close proximity. Therefore, the low-voltage and compact semiconductor UV sensor is always the welcoming device.

Aside from the flame detection, the installation of fire alarm systems may be constrained. For example, in ancient and historic buildings, the construction works of the cable layout for wired fire alarm systems may damage the building architecture and decoration, which are usually unrecoverable. A wireless sensor network (WSN) with flame detectors as WSN nodes [8]–[10] can alleviate this problem with no wiring network installation. Furthermore, its ad hoc infrastructure offers high flexibility in sensor placement and needs no particular human control and intervention [11]–[14]. The sensor nodes are self-organized to gather in real time the environmental data and detect abnormalities in the monitoring region. A large number of sensor nodes can also be organized in piconet so as to extend the coverage area. In a wireless sensing network for fire safety, there is a tacit assumption of a tiny WSN node with low power consumption. It is still rare to have such a WSN node in the reviewed literatures.

In this context, this paper reports a WSN node for fire safety, and we first characterize the emission spectrum from flames using a spectroscopic technique. Radiations from a common hydrocarbon flame are analyzed and used as the flame reference of this study. The discussion of the fabrication of the ZnSSe UV photodetector is then followed. It utilizes the state-of-the-art semiconductor-based nanotechnology, enjoying the merit of low cost, compact size, and high reliability. Furthermore, no external bias is required, saving power consumption and extending the device lifetime. There is also no inter-interfering effect as in UV flame detectors using the Geiger–Müller counter. Finally, the aforementioned ZnSSe UV photodetector is integrated with a ZigBee transceiver so as to implement a

Manuscript received September 23, 2010; revised November 30, 2010 and January 24, 2011; accepted January 27, 2011. Date of publication February 24, 2011; date of current version September 7, 2011.

P. Cheong, K.-F. Chang, S.-K. Ho, and K.-W. Tam are with the Faculty of Science and Technology, University of Macau, Macau 999078, China (e-mail: pcheong@umac.mo; fstkafai@umac.mo; phoebeho@umac.mo; kentam@umac.mo).

Y.-H. Lai and I.-K. Sou are with the Nano Science and Technology Program and Department of Physics, The Hong Kong University of Science and Technology, Kowloon, Hong Kong.

Color versions of one or more of the figures in this paper are available online at http://ieeexplore.ieee.org.

Digital Object Identifier 10.1109/TIE.2011.2119455

compact WSN node for fire safety. Additional signal processing is developed for high gain for example.

II. Flame Characterization Using Emission Spectroscopy

A. Flame Emission Spectroscopy

Emission spectroscopy is one of the promising techniques for flame analysis since it can provide valuable insights in the flame process [15]–[17]. Emission would not only be affected by radical and gas mixture, but the gas purity and gas flow will also influence the captured spectrum. Thus, various information of the combustion system can be revealed by optical emissions.

The emission spectrum from flames can be classified as continuous and discontinuous spectra. Continuous spectra occurred in all wavelengths within a certain domain. In a combustion system, they are generally observed in the sooty region of rich hydrocarbon flames. The continuous emission may be attributed to processes as the recombination of ions or associations of atoms and radicals. In contrast to the continuous manner, the spectral feature of discontinuous spectra is with a narrow wavelength, and it is mainly due to emission from isolated atoms and molecules. Specifically, the spectra that were attributed by free atoms are called atomic spectra; emissions from free molecules compose molecular spectra.

In flame, ordinary molecules are not stable products, such as H_2O, CO_2, CO, O_2, or N_2, and they change their states due to transition from one configuration of electrons of a molecule to another configuration. This change of electronic energy will result in emission with appreciable strength in visible and UV regions [18]. Therefore, the detection of UV emission from flame is of particular interest [19]. In this connection, a UV WSN node for flame detection is proposed and demonstrated in this paper. Before reporting the implementation of this WSN node, results of emission spectra for candle flame will be presented in the following section. The optical emission of flame from candle wax is a typical source, and the results would help in the characterization for some elements in the flame within the UV region.

B. Experiment for Candle Flame Characterization

The detection of UV emission was accomplished by a spectrograph (Dongwoo 500i) and an intensified charged-coupled device (ICCD, Andor iStar DH734). The spectrograph was for the wavelength selection of the signal and was controlled by a computer. Three gratings of 150, 600, and 2400 l/mm were equipped, and their wavelength ranges at 435.8 nm are 175, 43, and 8.6 nm, respectively. An ICCD was used for the detection of emission. It was triggered internally, and the settings were controlled by Andor software. In this paper, the emission spectra for candle flame were captured with accumulations of 100 events, an integration time of 10 ms, and an intensifier gain of 50. These experimental conditions are selected in order to prevent the saturation of signals while preserving perceptible emission intensity. All the displayed spectra were background corrected and smoothed with a 15-pixel sliding average. The instrumental resolution was well preserved after data processing.

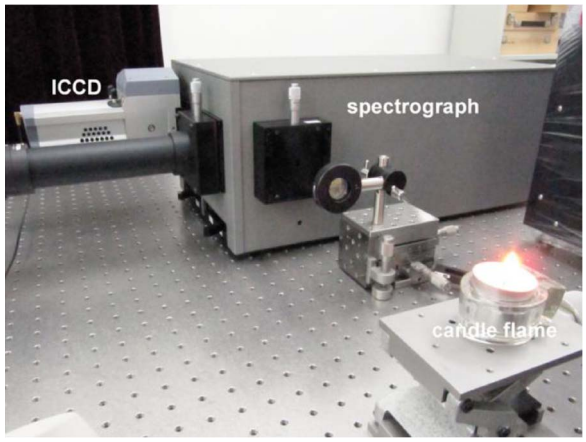

Fig. 1. Experimental setup for capturing emission spectra from candle flame.

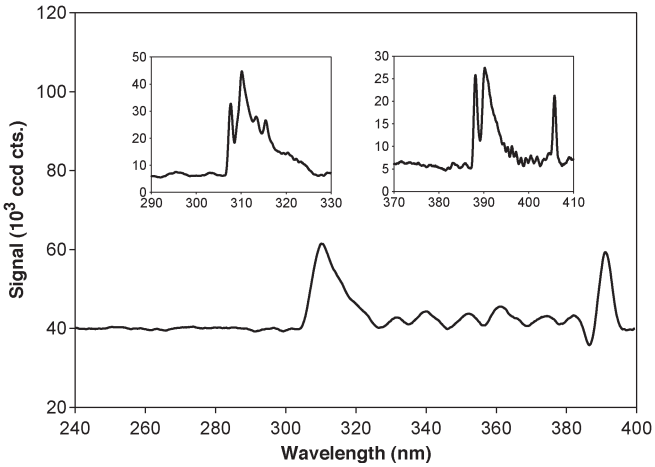

Fig. 2. Panoramic scans of emissions of candle flame in UV region. Insets show emission spectra of OH (hydroxyl) and CH (hydrocarbon) radicals.

The photograph of the experimental setup was shown in Fig. 1. The luminous lights from 30 cm were imaged onto the entrance slit of a 0.5-m spectrograph by a lens of fused silica with a focal length of 100 mm. Fused silica lens was used because of its high transmittance in the UV range. Depending on the required resolution and wavelength range, either 150-l/m or 600-l/mm gratings was used. The slit width was set to 200 μm. Emission signals were then detected by the ICCD mounted on the exit plane of the spectrograph.

C. Result and Discussion

Fig. 2 shows the emission spectrum captured from the candle flame in the UV region from 230 to 400 nm by a 150-l/mm grating. Noticeable signals can be clearly seen and were emitted in a continuous behavior. It was found that the UV light emerged as the continuum background.

In addition to the features from the UV emission continuum, some molecular spectral characteristics are expected since radiations from radicals are commonly found in visible and UV regions. In this regard, higher resolution spectra were then captured by a 600-l/m grating, and molecular features could be resolved.

The chemical composition of candle wax is $C_{25}H_{52}$. Its flame can produce the bands as in hydrogen flames and also emit radiation of hydrocarbon radicals. One of the insets in Fig. 2 shows the spectrum centered at 310 nm covering a range of 40 nm. It shows marked OH (hydroxyl) bands with the head at 306.4 nm [20]. The existence of the OH molecule in flames is proven through the UV bands, the strongest of which lies at 306.4 nm as can be seen in the figure. The excited OH radical OH^* can be formed in the primary combustion zone by the following chemiluminescent reaction [21]:

$$CH + O_2 \rightarrow CO + OH^*. \quad (1)$$

The subsequent process will be the decay of the excited hydroxyl radical to its ground state with emitted radiation. Aside from the OH bands that radiate from the primary combustion zone, another component is distinct in hydrocarbon flames, namely, CH bands at 387 and 432 nm [20]. Since UV emissions are involved in our proposed WSN node, thus, only the spectrum for the band at 387 nm is shown in the inset of Fig. 2. Moreover, the spectrum is taken in the visible wavelength range to validate the existence of the CH radical, and intense signals for the band at 432 nm are observed. The formation of excited CH may be by the following reactions:

$$C_2 + OH \rightarrow CO + CH^* \quad (2)$$

$$C_2H + O \rightarrow CO + CH^*. \quad (3)$$

As can be seen, excited CH may not be formed by the breakdown of molecules of wax directly, and C_2 can be an intermediate substance.

In summary, radiations from a common hydrocarbon flame of a candle are detected by emission spectroscopy. To aim the application of the proposed UV WSN node, only the region from 230 to 400 nm, covering from deep UV to long UV wavelength, is concerned. Results show that there are noticeable emissions in this wavelength range. Moreover, molecular features of OH and CH were apparent as radicals of the candle flame. Briefly, the detection of UV emissions as the evidence of the presence of flame is attainable for the fire safety issue.

III. ZnSSe UV Photodetector

The ZnSSe-alloy-based visible-blind UV detectors used in this paper were fabricated on an epi-ready 2-in device wafer on n^+-GaAs (100) substrates by the molecular beam epitaxy (MBE) technique using a VG V80H MBE system dedicated for the expitaxial growth of II–VI thin-film structures. Two effusion cells containing high-purity ZnSe and ZnS compounds, respectively, were used as the evaporation sources. The substrate was mounted on a molybdenum holder by liquid gallium. Right after being loaded into the growth chamber, the substrate was heated up to 580 °C to remove the protection oxide layer under the *in situ* reflection high-energy electron diffraction monitoring. This de-oxide heating also serves as a reliable process for achieving the back side ohmic contact of the substrate through its reaction with the liquid gallium. A thin layer of ZnSSe which acted as the active layer of the devices was then deposited directly onto the substrate with the substrate temperature set at 270 °C. The two effusion cells were set at 662 °C and 930 °C for the ZnSe and ZnS sources, respectively, and the growth lasted for 78 min. An alloy metallic thin film (a nondisclosure material) was then deposited also inside the MBE growth chamber, which acts as a Schottky metal layer on the ZnSSe active layer so as to form the metal–semiconductor Schottky-barrier photodiode devices [22].

After the 2-in device wafer was removed from the growth system, a standard photolithographic technique was used to define mesa structures to fabricate microdevices on the sample wafers. The bonding pads were fabricated by the thermal evaporation of a Cr (5 nm)/Au (800 nm) double layer with the Cr layer making direct contact with the Schottky metal to assure good adhesion.

A piece cut from the 2-in device wafer was handled by standard polishing and ion-milling techniques for cross-sectional transmission electron microscopy (TEM) structural characterization. TEM images were obtained by using a high-resolution JEOL 2010F TEM system operating with a LaB6 filament at 200 kV. The Se composition of the ZnSSe active layer was analyzed by an energy-dispersive X-ray spectroscopy (EDS) facility that was integrated with the TEM instrument. The results of the imaging and EDS studies reveal that the active ZnSSe layer is single crystalline, although high-density lattice-mismatch dislocation defects were observed near the interface between the active layer and the substrate. The thicknesses of the active layer and the Schottky metal layer were determined to be around 280 and 13 nm, respectively. The Se composition of the active layer was found to be around 10%.

Photoresponse measurements of the devices were carried out using a 150-W Xenon arc lamp as the light source and an ARC SpectraPro-275 scanning monochromator. For a wavelength shorter than 380 nm, a low-pass filter (UG11) was placed right above the device being measured to make sure the light shining on the device is free of unexpected long wavelength radiation exiting from the monochromator. For the wavelength equal and longer than 380 nm, a high-pass filter (L38) was used instead to avoid second-order effect. At each wavelength, the power of the light incident on the device was carefully measured using a Newport 835 optical power meter that uses a UV-enhanced Si photodiode (818UV) as the detector. The short circuit photocurrent I_{sc} was measured as a function of the wavelength of the incident photons using a digital current meter (Keithley Model 237) with high sensitivity and high precision.

Fig. 3 displays the measured photoresponse of the ZnSSe-based UV photodiode for the spectral region ranging from 300 to 700 nm. The cutoff wavelength, defined as the wavelength of which the response is about one order lower than the peak response, was found to be around 360 nm. As can be seen in Fig. 3, the long wavelength rejection at 700 nm is more than four orders. The small bumps that peaked at 400 and 500 nm are believed to be caused by unwanted impurities in the source materials during the MBE growth. A bare ZnSSe UV photodectector as shown in Fig. 4 was glued on an FR4 printed circuit board, and its terminals were connected with gold bonding wires.

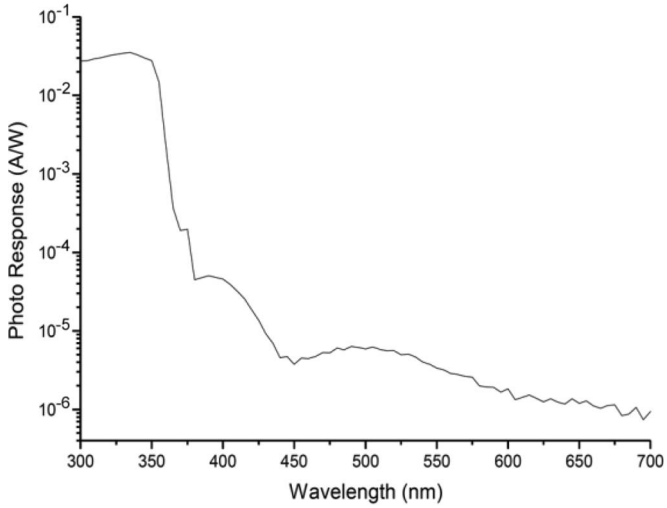

Fig. 3. Measured photoresponse of ZnSSe UV photodetector.

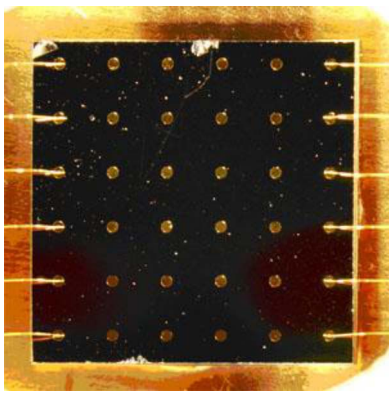

Fig. 4. ZnSSe UV photodetector.

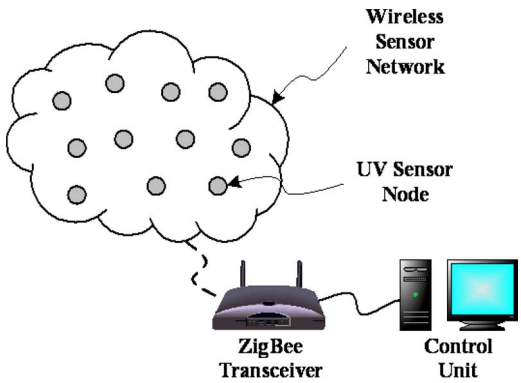

Fig. 5. ZigBee-based WSN for flame detection.

IV. ZigBee-Based WSN Node for UV Detection of Flame

A. Network Configuration

For fire safety, as shown in Fig. 5, a WSN configured in an ad hoc infrastructure is designed for the UV detection of flame. It includes the WSN node and a control center. The low-power-consumption short-range communication technology ZigBee is used, and it has 16 channels of data rate 250 kb/s in the license-free industrial, scientific, and medical band of 2.4–2.4835 GHz.

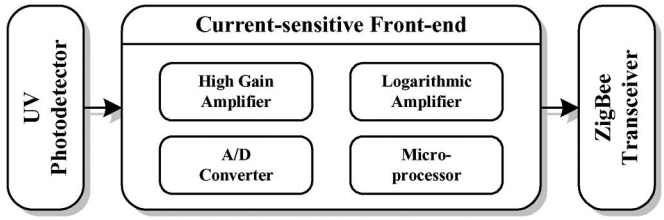

Fig. 6. WSN node for flame detection.

In each channel, the ZigBee supports 65 000 unique network addresses. Instead of the normal operation, the ZigBee module can be configured as low-power-consumption cyclic sleep mode for power saving. In order to increase the coverage of the flame detection, the peer-to-peer topology is selected instead of the point-to-multipoint topology. The former one can arbitrarily extend the distance between the WSN node and the control unit. In each node, the ZnSSe UV photodetector presented in Section III is integrated with a ZigBee transceiver module operated in a full function device (FFD). A control center also includes a ZigBee transceiver module in the FFD mode and a PC. A simple serial communication software application is programmed to monitor the status of the UV emission in the area of concern.

B. Node's Basics

In a sensor node, it mainly consists of three modules, namely, a ZnSSe UV photodetector, a current-sensitive front end, and a ZigBee transceiver as illustrated in Fig. 6. The ZnSSe UV photodetector fabricated in Section III can be modeled as a photodiode. It has a low-pass response for UV and cuts off at the 36-nm wavelength. The output dc current of the photodetector is directly proportional to the effective sensing area, and an area of 6×6 mm^2 is designed in our node. For wireless connectivity, the ZigBee transceiver module XBee from MaxStream is used, and it is operated in low 3.3-V dc supply voltage. Configuring the ZigBee transceiver in 0 dBm, the ZigBee transceiver module can cover 30 m indoor, and the flame detection coverage can be extended to 100 m for outdoor application [23]. For power saving purpose, this module is normally configured to cyclic sleep mode.

A current-sensitive front end is then designed to convert the picoampere dc output current of the ZnSSe UV photodetector into a digitalized signal as the input of the ZigBee transceiver. To process this low current, the high-performance operational amplifier (opamp) OPA128 from Texas Instruments [24] is used to achieve the current-to-voltage conversion. This opamp provides an extremely high gain of 120 dB, high input impedance ($> 10^{13}\ \Omega$), and also low offset current (< 65 fA) at the inputs. This circuit amplifies and converts the output current of photodetector $I_{\rm IN}$ to voltage $V_{\rm OUT}$ with the gain controlled by the feedback resistor $R_{\rm F}$ as illustrated in Fig. 7. A low-pass characteristic is performed due to the existence of the feedback capacitor $C_{\rm F}$. In our prototype, $R_{\rm F}$ and $C_{\rm F}$ are 100 MΩ and 33 nF, respectively. To this end, the picoampere input signal is enlarged to a satisfactory level (i.e., hundreds of millivolt to

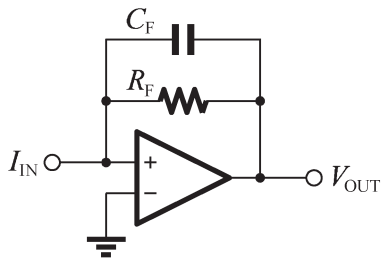

Fig. 7. Signal conditioner of WSN node.

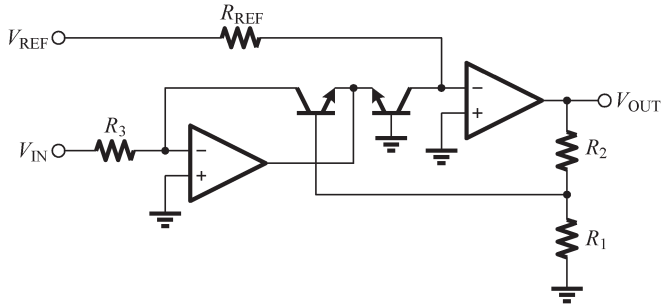

Fig. 8. Schematic of logarithmic amplifier.

volts) in addition to the capability of suppressing low frequency noise, for example, noise from the mains (50–60 Hz).

Following the high gain amplifier, a logarithmic circuit converts the output voltage from a linear scale to a logarithmic scale as shown in Fig. 8. It consists of two linear amplifiers, two NPN bipolar transistors, and a resistor ladder as depicted in Fig. 8. The sensitivity of this node for a weak UV signal is thus increased, for example, a small signal range of 1 mV to 10 V is converted into 50-dB scales, with $V_{\mathrm{REF}} = 1.25$ V, $R_{\mathrm{REF}} = 1.1\ \mathrm{M}\Omega$, $R_1 = 100\ \Omega$, $R_2 = 730\ \Omega$, and $R_3 = 10\ \mathrm{k}\Omega$. In the prototype, the operating current is measured as 7.3 mA. In addition, the logarithmic amplifier transforms the voltage into a logarithmic scale with

$$V_{OUT} = 0.5 \log(V_{IN}) + 1. \tag{4}$$

For mixed-signal data processing, an analog-to-digital converter (ADC) controlled by a microprocessor is used. As the logarithmic amplifier increases the sensitivity in a weak UV signal, a less stringent 8-b ADC with a full scale of 1.25 V and a sampling data rate of 100 kb/s is chosen to provide a good resolution (5 mV/step). Also, the microprocessor sends the sampled data to the ZigBee transceiver module through the UART interface. The nominal communication speed between the signal conditioner and the ZigBee transceiver module is set at 9600 b/s within a 70-ms data sampling period.

V. Measurement Results

To validate the proposed wireless flame sensing, we have designed and prototyped a WSN node as shown in Fig. 9, including a ZnSSe UV photodetector, a current-sensitive front end, and a ZigBee transceiver. This prototyped sensor node is measured as $9 \times 6\ \mathrm{cm}^2$. A cyclic sleep mode of the prototype is adopted with a duty cycle of 0.17%. Under this power saving

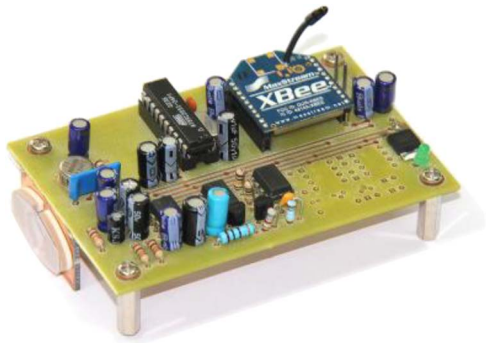

Fig. 9. Photograph of the sensor node prototype.

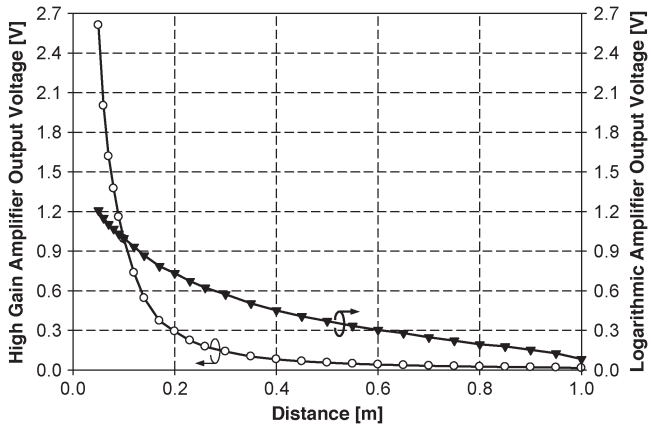

Fig. 10. Change in output voltages of high gain amplifier (—○—) and logarithmic amplifier (—▼—).

scheme, the average current consumption (within a period) is recorded as 700 μA.

In order to ease the measurement, this experiment is carried out in an indoor environment with the candle flame shown in Fig. 1 as the UV source. The background noises, including sunlight and indoor lightings, are cancelled out for characterization with a "dummy" WSN. It should be noticed that direct exposure to the sunlight will affect the accuracy of UV sensing. Nevertheless, in our experimental setup, the weak signal (UV) strength from a candle flame helps to analyze the sensitivity of the prototype within a short distance (< 1 m). When a luminous flame was imaged onto the node in different angles, the node's output was then measured at a fixed distance. Contrarily, its response was characterized by different distances for some luminous angles. In the aforementioned two measurements, the detection time, including the ZigBee transmission and data processing, is as quick as 70 ms.

A. Response of WSN Node at Different Luminous Distances

Fig. 10 recorded the measured output voltages of the high gain amplifier and the logarithmic amplifier, respectively, and a candle is used as the UV source in this experiment. These amplifiers provide a total of 174-dB gain for the node, and the logarithmic amplifier transforms the signal as (4).

From the figure, it can be observed that the output voltages drop as the distance between the UV WSN node and the candle

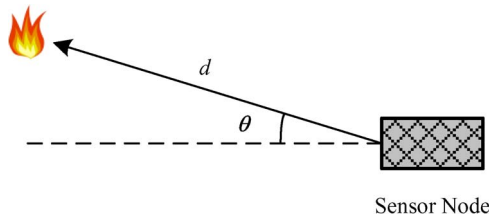

Fig. 11. Top view of experimental setup for flame's UV strength measurements.

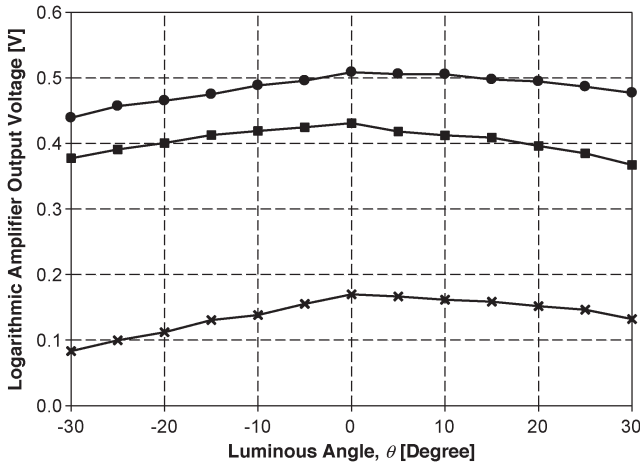

Fig. 12. Change in output voltages of logarithmic amplifier with different angles and distances ((−●−) 0.1 m; (−■−) 0.2 m; (−×−) 0.3 m).

increases. When the distance is small (< 0.2 m), the change in the high gain amplifier output voltage is obvious. It drops from 2.61 to 0.29 V as the distance increases. On the other hand, the change in the output of the logarithmic amplifier is comparatively small. It varies from 1.21 to 0.73 V.

When the distance exceeds 0.4 m, the high gain amplifier output voltage varies in a narrow range which is smaller than 0.08 V. If the distance further increases to 0.9 m, the output voltage reaches 0.02 V. The sensitivity will be limited if the high gain amplifier output voltage is sampled directly. In contrast, the logarithmic amplifier has the output voltages of 0.73 and 0.15 V at 0.4 and 0.9 m, respectively. It is clear that the sensitivity for weak signal strength is highly increased due to the existence of the logarithmic amplifier. In consequence, the requirement of the ADC is greatly relaxed.

B. Response of WSN Node at Different Luminous Angles

In contrast to the distance measurement, the response of the prototype node is studied at different luminous angles. The experimental setup is depicted in Fig. 11, and the results are illustrated in Fig. 12, respectively. Three different distances, 0.1, 0.2, and 0.3 m, were used to investigate the responses. As expected, the sensor node has the largest readings as the candle is placed in an incident angle ($\theta = 0^\circ$). When the angle increases or decreases, the UV strength drops significantly. For example, when the distance is 30 cm and the luminous angle is -30°, the UV strength decreases from 0.17 to 0.08 V, which is equivalent to a 53% signal reduction.

VI. Conclusion

This paper has presented a low-cost and low-power ZigBee-based WSN node for the UV detection of flame, contributing to the fire safety protection industry. A prototype node includes a tiny passive ZnSSe UV photodetector; a current-sensitive front end, including a total of 174-dB gain from the combination of a high-gain current-to-voltage amplifier and a logarithm converter with 50-dB scales; and a low-power-consumption 2.4-GHz ZigBee transceiver. A fabricated photodetector is designed to have a cutoff at 360 nm to convert the UV emission of flame into picoamperes. Including mixed signal processing and ZigBee communications, the speed of reliable flame detection is as fast as 70 ms. The sensor node consumes only 2.3 mW from a 3.3-V supply in average. The presented flame detection can be easily integrated with building or facility management systems at low cost.

References

[1] D. Starikov, C. Boney, R. Pillai, and A. Bensaoula, "Dual-band UV/IR optical sensors for fire and flame detection and target recognition," in *Proc. ISA Sensors Ind. Conf.*, 2004, pp. 36–40.
[2] L. Xu and Y. Yan, "A new flame monitor with triple photovoltaic cells," *IEEE Trans. Instrum. Meas.*, vol. 55, no. 4, pp. 1416–1421, Aug. 2006.
[3] B. U. Toreyin, E. B. Soyer, O. Urfalioglu, and A. E. Cetin, "Flame detection using PIR sensors," in *Proc. 16th IEEE Signal Process., Commun. Appl. Conf.*, 2008, pp. 1–4.
[4] A. R. Pauchard, D. Manic, A. Flanagan, P. A. Besse, and R. S. Popovic, "A method for spark rejection in ultraviolet flame detectors," *IEEE Trans. Ind. Electron.*, vol. 47, no. 1, pp. 168–174, Feb. 2000.
[5] Z. Djurić, K. Radulović, N. Trbojević, and Ž. Lazić, "Silicon resonant cavity enhanced UV flame detector," in *Proc. 23rd Int. Conf. Microelectron.*, 2002, pp. 239–242.
[6] R. C. Luo and K. L. Su, "Autonomous fire-detection system using adaptive sensory fusion for intelligent security robot," *IEEE/ASME Trans. Mechatronics*, vol. 12, no. 3, pp. 274–281, Jun. 2007.
[7] Hamamatsu Photonics K.K., Electron Tube Division, 2010 Photonic Devices: Electron Tube Devices and Applied Products, p. 24, Iwata City, Japan, 2001.
[8] L. Ferrigno, A. Pierosanto, and V. Paciello, "Low-cost visual sensor node for bluetooth-based measurement networks," *IEEE Trans. Instrum. Meas.*, vol. 55, no. 2, pp. 521–527, Apr. 2006.
[9] G. Boggia, P. Camarda, L. A. Grieco, and M. R. Palattella, "Fire detection using wireless sensor networks: An approach based on statistical data modeling," in *Proc. New Technol. Mobility Security*, 2008, pp. 1–5.
[10] S. Liu, D. Tu, and Y. Zhang, "Multiparameter fire detection based on wireless sensor network," in *Proc. Int. Intell. Comput. Intell. Syst. Conf.*, 2009, pp. 203–206.
[11] X.-H. Cao, J.-M. Chen, Y. Xiao, and Y.-X. Sun, "Building-environment control with wireless sensor and actuator networks: Centralized versus distributed," *IEEE Trans. Ind. Electron.*, vol. 57, no. 11, pp. 3596–3605, Nov. 2010.
[12] J. P. Carmo, P. M. Mendes, C. Couto, and J. H. Correia, "A 2.4-GHz CMOS short-range wireless-sensor-network interface for automotive applications," *IEEE Trans. Ind. Electron.*, vol. 57, no. 5, pp. 1764–1771, May 2010.
[13] B. Lu and V. C. Gungor, "Online and remote motor energy monitoring and fault diagnostics using wireless sensor networks," *IEEE Trans. Ind. Electron.*, vol. 56, no. 11, pp. 4651–4659, Nov. 2009.
[14] V. C. Gungor and G. P. Hancke, "Industrial wireless sensor networks: Challenges, design principles, and technical approaches," *IEEE Trans. Ind. Electron.*, vol. 56, no. 10, pp. 4258–4625, Oct. 2009.
[15] V. Gautam and A. K. Gupta, "Spectroscopic analysis of fuel lean flames for propulsion applications," in *Proc. ASME Power*, 2004, pp. 495–504.
[16] M. Ghaderi and A. K. Gupta, "Spectroscopic analysis of diffusion flame using high temperature combustion air," in *Proc. ASME Power*, 2004, pp. 591–603.
[17] O. Farias and P. Ngendakumana, "Flame spectroscopy and the NOx formation mechanisms in fuel oil boilers," *Bull. Soc. Chim. Belges*, vol. 105, no. 9, pp. 545–554, Dec. 1996.

[18] W. Hwang, J. Dec, and M. Sjoberg, "Spectroscopic and chemical-kinetic analysis of the phases of HCCI autoignition and combustion for single- and two-stage ignition fuels," *Combustion Flame*, vol. 154, no. 3, pp. 387–409, Aug. 2008.
[19] R. Obertacke, H. Wintrich, and F. Wintrich, "A new sensor system for industrial combustion monitoring and control using UV emission spectroscopy and tomography," *Combustion Sci. Technol.*, vol. 121, no. 1–6, pp. 133–151, 1996.
[20] J. Kojima, Y. Ikeda, and T. Nakajima, "Spatially resolved measurement of OH^*, CH^*, and C_2^* chemiluminescence in the reaction zone of laminar methane/air premixed flames," *Proc. Combustion Inst.*, vol. 28, no. 2, pp. 1757–1746, 2000.
[21] S. W. Yoo, C. K. Law, and S. D. Tse, "Chemiluminescent OH^* and CH^* flame structure and aerodynamic scaling of weakly buoyant, nearly spherical diffusion flames," *Proc. Combustion Inst.*, vol. 29, no. 2, pp. 1663–1670, 2002.
[22] I. K. Sou, Z. H. Ma, and G. K. L. Wong, "Photoresponse studies of ZnSSe visible-blind UV detectors: A comparison to ZnSTe detectors," *Appl. Phys. Lett.*, vol. 75, no. 23, pp. 3707–3709, Dec. 1999.
[23] Digi Int. Inc., Datasheet: XBee/XBee-Pro OEM RF Modules, Minnetonka, MN.
[24] Texas Instruments, Datasheet: OPA128 Difet Electrometer-Grade Operational Amplifier, Mansfield, TX.

Pedro Cheong (S'98) received the B.Sc. and M.Sc. degrees in electrical and electronics engineering from the University of Macau, Macau, China, in 2000 and 2005, respectively, where he is currently working toward the Ph.D. degree.

He is currently a Laboratory Technician with the Radio Frequency Integrated Circuits and Systems Laboratory, University of Macau. He has published more than 20 referred journals and conference papers. His research interests include RF/microwave passive filter modeling and design, active RF integrated circuit component designs, wireless sensor network, and beamforming techniques for smart antennas.

Ka-Fai Chang (M'10) received the B.Sc. (with first-class honors) and M.Sc. degrees in electrical and electronics engineering from the University of Macau, Macau, China, in 2000 and 2004, respectively, and the Ph.D. degree in electronic engineering from The Chinese University of Hong Kong, Hong Kong, China, in 2011.

He is currently with the University of Macau. His research interests include frequency synthesizer and RF/microwave passive and active circuit designs.

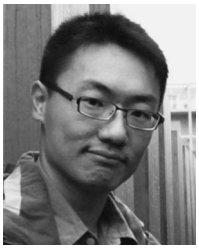

Ying-Hoi Lai was born in Hong Kong. He received the B.Sc. and M.Phil. degrees from The Hong Kong University of Science and Technology, Kowloon, Hong Kong, in 2006 and 2009, respectively, where he is currently working toward the Ph.D. degree.

Since 2009, he has been with the Nano Science and Technology Program, The Hong Kong University of Science and Technology. His research interests include molecular beam epitaxial growth, characterization of II–VI semiconductors, and UV optoelectronic devices.

Sut-Kam Ho was born in Macau, China, in 1974. She received the B.Eng. degree in electrical and electronics engineering from the University of Macau, Macau, in 1995, the B.Sc. and M.Phil. degrees in physics from The Hong Kong University of Science and Technology, Kowloon, Hong Kong, in 1997 and 1999, and the Ph.D. degree in physics from Hong Kong Baptist University, Kowloon, in 2007.

Since 1997, she has been an Assistant Professor with the Faculty of Science and Technology, University of Macau. Her research interests include laser material interaction, spectroscopy, and trace analysis. She pioneered an analytical technique of plume laser-excited atomic fluorescence which is capable of highly sensitive elemental analysis and successfully applied this tool for the analysis of aqueous and solid samples. Moreover, she used laser spectroscopy to analyze gemstones with minimal destruction of samples.

Dr. Ho is a member of the Society of Applied Spectroscopy in the U.S. and an active member of a few local science promotion programs.

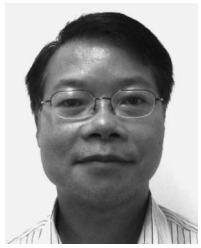

Iam-Keong Sou received the Ph.D. degree in physics with his thesis research on dopant incorporation and transport properties of molecular beam epitaxy-grown HgCdTe-based quantum structures from the University of Illinois at Chicago, Chicago, in 1990.

He joined The Hong Kong University of Science and Technology (HKUST), Kowloon, Hong Kong, as a Faculty Member in 1991 and is currently a Full Professor in the Department of Physics, HKUST. He served as the Vice President of The Physical Society of Hong Kong in the period of 2001–2005. He has published more than 160 refereed papers and is currently the holder of three U.S. patents, one Australian patent, and one Chinese patent. He and his collaborators pioneered a visible/solar-blind UV detector technology that has reached a fully commercialization stage with a mass-production scale. The developed UV sensors have been widely adopted in several consumer products such as wrist watches, walkie talkies, sunglasses, testers, and air pollution monitors. Potentially, the solar-blind UV sensors could also act as a critical component in the flame sensor market and a number of medical applications. His current research focuses on the growth mechanisms and applications of a number of novel low-dimensional nanostructures, including semiconductor and metallic quantum dots, nanowires, nanotrenches, and nanogratings as well as the novel properties of the Bi_2Te_3 topological insulator.

Kam-Weng Tam (S'91–M'01–SM'05) was born in Macau, China, in 1969. He received the B.Sc. degree in electrical and electronics engineering from University of Macau, Macau, the joint Ph.D. degree in electrical and electronics engineering from the University of Macau and the Technical University of Lisbon, Lisbon, Portugal, in 1993 and 2000, respectively.

From 2000 to 2001, he was the Director with Instituto de Engenharia de Sistemas e Computadores, Macau. In 2001, he cofounded the first microelectronic design house in Macau, where he was also the General Manager until 2003. He is currently an Associate Professor of the University of Macau. His research interests have been on microwave circuits, radio frequency identification, smart antennas, wireless sensors, and monolithic microwave integrated circuits. He pioneered many wireless applications in Macau, namely, UHF RFID Library Automation, Wireless Flame Sensor, and so forth. He has published one book chapter and more than 100 referred papers.

Dr. Tam was the recipient of the Institute of Electrical, Information and Communication Engineers Communications Society Distinguished Contributions Award in 2009 and was the advisor of two recipients of the IEEE MTT-S Undergraduate Scholarship in 2002 and 2003. He served as an Interim Secretary for the formation of the IEEE Macau Section in 2003 and was the Founder of the IEEE Macau AP/MTT Joint Chapter in 2010, where he also serves as the Chair from 2011 to 2012. He was the Vice Chair of the Asia-Pacific Microwave Conference 2008, the Technical Program Cochair of the IEEE MTT-S International Microwave Workshop Series on Art on Miniaturizing RF and Microwave Passive Components 2008, and the General Cochair of the International Symposium on Antennas and Propagation 2010.